Catal Lett (2013) 143:375–385
DOI 10.1007/s10562-013-0987-5

PERSPECTIVE

Towards Realistic Surface Science Models of Heterogeneous Catalysts: Influence of Support Hydroxylation and Catalyst Preparation Method

Martin Sterrer · Hans-Joachim Freund

Received: 19 February 2013 / Accepted: 25 February 2013 / Published online: 12 March 2013

Abstract Surface science studies allow processes important for heterogeneous catalysis to be investigated in greatest detail. Starting from the simplest model of a catalytic surface, a metal single-crystal surface under ultrahigh vacuum conditions, enormous progress has been made in the last decades towards extending the surface science of catalysis to technically more relevant dimensions. In this perspective, we highlight recent work, including our own, dealing with the influence of water on metal-support interactions in surface science studies of oxide-supported metal nanoparticle model catalysts. In particular, the effect of hydroxyl groups on nucleation and sintering of metal nanoparticles, and surface science investigations into catalyst preparation using wet-chemical procedures are addressed.

Keywords Heterogeneous catalysis < catalysis · Oxide supports < preparation and materials · Metal-support interaction < preparation and materials · Characterization < methodology and phenomena · Thin films < methodology and phenomena · Spectroscopy and general characterisation

M. Sterrer (✉) · H.-J. Freund
Department of Chemical Physics, Fritz-Haber-Institut der Max-Planck-Gesellschaft, Faradayweg 4–6, 14195 Berlin, Germany
e-mail: sterrer@fhi-berlin.mpg.de

H.-J. Freund
e-mail: freund@fhi-berlin.mpg.de

1 Introduction

Molecular level details are difficult to obtain from industrially applied heterogeneous catalyst materials because of their structural and chemical complexity. Instead, one must resort to simplified models such as "dispersed model systems" (powders), which will not be further discussed here, or planar model systems that allow sophisticated surface characterization techniques to be applied. The "classical" surface science approach, which also represents the simplest model approach in terms of surface structure, uses metal single-crystal surfaces in combination with the power of available ultrahigh vacuum (UHV)-based microscopic and spectroscopic techniques to gain detailed atomic and molecular level understanding of catalytically relevant processes such as adsorption, diffusion and reaction, and their structure sensitivity [1–3]. This approach has, however, two main limitations, which are commonly referred to as pressure gap and materials gap: first, adsorption structures and reaction pathways observed under UHV conditions may not necessarily be the same as those present under realistic pressure conditions. And second, single-crystal metal samples do not cover important materials aspects of a technical catalyst such as particle size effects and the influence of the support. Therefore, several approaches have in recent years been put forward in order to overcome these limitations [4–6].

New developments in experimental techniques enabled in situ studies under elevated pressure conditions. These include, for example, photon-based techniques such as polarization-modulation infrared reflection absorption spectroscopy (PM-IRAS) or sum frequency generation for vibrational spectroscopic characterization [7], ambient pressure X-ray photoelectron spectroscopy (AP-XPS) for electronic structure characterization [8], and high-pressure

scanning tunneling microscopy (HP-STM) for morphological characterization [9].

With the objective to include the influence of the oxide support as well as particle size effects, the surface science approach has been extended to model systems with increased materials complexity such as those represented by metal particles supported on flat oxide substrates [10–14]. A particular appealing approach in this respect is the utilization of thin, single-crystalline oxide films grown on metallic substrates as support for catalytically active metal nanoparticles. Because these support materials exhibit finite electrical conductivity even if the oxide in its bulk form has a large band gap, UHV-based analytical tools that rely on charged information carriers (electrons, ions) can be applied in a similar way as for metallic samples, allowing atomic scale information of surface processes on these model catalysts to be obtained [15]. As an example, an MgO(100)-supported Au thin film model system and the individual stages of preparation viewed with STM is presented in Fig. 1.

This particular example serves to demonstrate the enormous potential of the thin film model approach for providing fundamental understanding of the surface properties. For Au/MgO(001), the combination of several experimental techniques, in particular STM, electron spin resonance (ESR), IRAS and temperature programmed desorption (TPD), with computational studies using density functional theory (DFT), allowed the properties of the oxide surface, of metal atoms adsorbed on the oxide surface [17], as well as of point defects on the oxide surface [18, 19] and their interaction with metal atoms and particles [20] to be determined at the atomic scale.

The surface science approach to catalysis using oxide-supported metal nanoparticles and applying UHV as well as in situ characterization techniques has certainly contributed to deepen the understanding of processes in heterogeneous catalysis and provided also fundamental insight into the interaction of metal atoms and nanoparticles with the support material. The success of this approach is also based on the fact that UHV methodologies allow these model systems to be prepared and studied under ultra-clean, contaminant-free conditions, which greatly simplifies the interpretation of results. In spite of the huge achievements in terms of materials complexity and realistic reaction conditions in the field of model catalysis, there still remain some open questions regarding the comparability to real-world catalyst materials. Among them are (i) the influence of surface functionalization of the support and (ii) the influence of the catalyst preparation method.

2 Influence of Surface Hydroxyls on Metal Nucleation

Consider first the support functionalization: Any technical catalyst will get in contact with ambient at some particular stage of its lifetime and, therefore, expose a different surface functionality as compared to a clean model catalyst in UHV. The most important surface modification in this respect is certainly hydroxylation of the oxide support. The importance of hydroxyl groups is well appreciated in the applied catalysis community [21]. On the other hand, rather little work has been done, especially with respect to surface hydroxylation at relevant water partial pressures and the subsequent interaction of deposited metals with hydroxyls, from a surface science point of view.

An important aspect that needs to be considered first is the hydroxylation state of an oxide surface, which depends on the type of the oxide and its surface orientation, as well as on the chemical potentials of water and oxygen. For example, dissociative adsorption of water is thermodynamically unfavorable on the stoichiometric surfaces of both TiO_2(110) and MgO(100) [22–24], but readily occurs on defects sites such as step edges or oxygen vacancies [23, 25, 26]. In contrast to TiO_2(110), which seems to be rather stable even in ambient environments and when contacted with liquid water [24, 27, 28], the MgO(100) surface becomes fully hydroxylated by exposure to water vapor in

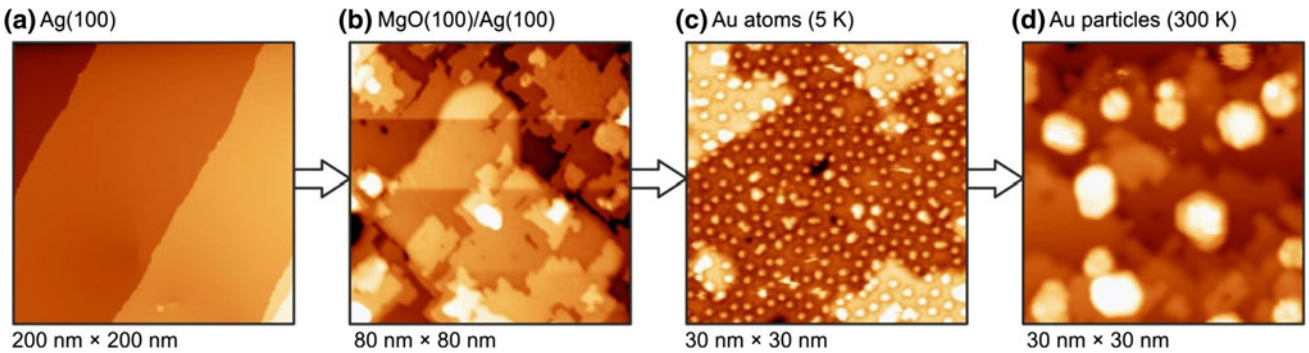

Fig. 1 Low-temperature (5 K) STM images of the various stages of Au/MgO(001)/Ag(001) model catalyst preparation. **a** Clean Ag(001) surface; **b** 8 ML MgO(001)/Ag(001) prepared by reactive deposition of Mg on Ag(001) in oxygen background. **c** Single Au atoms deposited at 5 K on a 8 ML MgO(001)/Ag(001) film. **d** Au particles on 8 ML MgO(001)/Ag(001) formed after annealing to 300 K. [16]

the mbar pressure range [29, 30]. For thermodynamic reasons, the hydroxylation of MgO(100) cannot be explained by water dissociation on cation–anion pairs on the (100) surface. Instead, it is assumed that the hydroxylated state is stabilized via Mg–O hydrolysis and a partial detachment of hydroxylated Mg^{2+} ions [31]. In contrast to TiO_2(110) and MgO(100), the surfaces of corundum-type oxides (e.g., α-Al_2O_3(0001), α-Fe_2O_3(0001)), which are terminated by a single metal layer in UHV, readily dissociate water at low pressures. At environmentally more relevant conditions (high oxygen or water chemical potential), these surfaces are terminated by an oxygen layer and become fully hydroxylated in the presence of water [32–35]. In the case of α-Al_2O_3(0001), the transformation into the hydroxylated state involves the hydrolysis of Al–O bonds and the formation of a gibbsite ($Al(OH)_3$)-like surface structure [36]. From these examples it is obvious that not only the hydroxyl coverage, but also the nature and the chemical properties of hydroxyls, and consequently, the surface reactivity may strongly depend on the environmental conditions.

In the most favorable situation, hydroxyl species formed on a single-crystalline oxide surface can be directly observed with microscopic techniques such as STM or atomic force microscopy. As an example that has been extensively treated in the literature, the formation of hydroxyl species by water dissociation at oxygen vacancies on a TiO_2(110) surface is listed. This process yields two similar OH species, commonly referred to as OH_{br} or H_{cap}, on the bridging oxygen rows on TiO_2(110) [26], which appear in STM as protrusions with slightly enhanced contrast as compared to oxygen vacancies [37, 38]. In a recent report, Matthey et al. [39] compared the nucleation and sintering of gold on hydrogenated TiO_2(110) with that on the corresponding reduced (containing O_{br} vacancies) and oxidized (containing O adatoms) TiO_2(110) surfaces. This study indicated that agglomeration of gold into large particles is facilitated by the small diffusion barrier of gold atoms on the hydrogenated surface, while on the reduced and oxidized surfaces the large trapping potential of O_{br} vacancies and O adatoms, respectively, leads to the stabilization of small Au clusters. The experimental findings were corroborated by DFT computations, which have in addition shown that the adhesion of Au clusters is significantly enhanced on the oxidized TiO_2(110) surface due to charge transfer [39]. On the other hand, a previous computational study demonstrated that the presence of terminal OH (OH_{tr}) groups adsorbed on the 5-fold coordinated Ti^{4+} on TiO_2(110) leads to a similar strong adhesion of Au particles as in the case of a surface modified by O adatoms [40]. While experimental verification of this result is probably difficult because of the weak thermal stability of OH_{tr} [41], it clearly highlights the influence of the type and chemical properties of OH groups on the stabilization of small Au particles.

A different way to introduce hydroxyl groups onto an inert oxide surface under UHV conditions can be realized by dissociation of water on pre-deposited metal adatoms [42–44]. In a set of experiments carried out in our laboratory, this methodology was applied to hydroxylate the surface of a thin alumina film grown on NiAl(110) by water dissociation on Al adatoms, and to further study the influence of hydroxyls on the properties of Rh particles deposited onto the modified oxide surface. For this particular example the results of a set of experimental techniques have consistently shown that (i) the Al adatoms are completely oxidized after water dissociation and the hydroxyl groups formed during this process are homogeneously distributed across the surface, (ii) the hydroxyls are consumed by deposited Rh atoms leading to the formation of oxidized Rh particles, and (iii) in comparison with Rh deposited on a pristine alumina film a higher nucleation density as well as sinter stability of the Rh particles is achieved on the hydroxylated alumina film [42, 45, 46].

Subsequently, a number of reports appeared that used α-Al_2O_3(0001) single-crystal surfaces in order to study the effect of hydroxyls on the properties of deposited metals [47–51]. For the metals studied (Co, Cu, Ti) a picture that is consistent with our conclusions from the Rh/alumina system was derived, namely that the metal adhesion to the hydroxylated surface is generally stronger as compared to the non-hydroxylated one, and that the deposited metal becomes oxidized according to

$$\left\{Al^{3+}OH^{-}\right\} + Me^{0} \rightarrow \left\{Al^{3+}O^{2-}\right\}Me^{+} + H \qquad (1)$$

The Cu/α-Al_2O_3(0001) system has led to some controversy in the past because model calculations indicated that a fully hydroxyl-terminated α-Al_2O_3(0001) binds a Cu overlayer weaker than the stoichiometric surface [52]. Better agreement with the experimental results was then obtained by considering only partially hydroxylated α-Al_2O_3(0001) and the interaction with single Cu atoms [53], which again underlines the fact that the interaction of metals with hydroxylated oxide surfaces may critically depend on the structure of the oxide surface and on the degree of hydroxylation, but also on metal coverage.

The consumption of hydroxyls by metals raises some questions about the fate of hydrogen that is supposed to be released as a result of reaction (1). To the best of our knowledge, hydrogen desorption has up to date not been reported in single-crystal model studies as described above. On the other hand, a number of computational studies carried out for metal clusters interacting with hydroxylated zeolite and γ-alumina models indicate that reverse spillover of hydrogen from surface OH groups onto (or into) the metal clusters is energetically more favorable than direct

H_2 desorption [54–56]. While experimental evidence for this process exists for a Rh/zeolite system [54, 57], further proof from flat surface science models is still pending.

For the last example to be discussed in this section, we return to the interaction of gold with surface hydroxyls and our most recent studies that used MgO(100) films grown on Ag(100) as support [58, 59]. The choice of gold was motivated by several reasons: first, the charge state of gold and the influence of surface hydroxyls in CO oxidation over supported gold catalysts has long been a matter of debate [60, 61]; second, high CO oxidation activity has been observed over gold supported on hydroxides (e.g., $Mg(OH)_2$, $La(OH)_3$, $Fe(OH)_3$) [62–66]; third, enhanced stability towards thermal sintering (and higher CO oxidation activity) was observed for gold over heavily hydroxylated (NaOH-treated) titania support as compared to non-treated one [67]; and finally, given the poor stability of oxidic gold species, it would be interesting to see if the interaction of gold with surface hydroxyls follows a similar pathway as described above (Eq. 1).

Prior to the metal nucleation study, the interaction of water with pristine MgO(100) films has been studied in detail. This included investigations into the structure of ordered water monolayers on MgO(100) [68], the wetting behavior of water ice [69], as well as the hydroxylation of the surface as a function of water partial pressure [30]. As to the latter, we present in Fig. 2 infrared spectra obtained after hydroxylation of MgO(100) films with D_2O vapor at room temperature. The spectral detail around 2,750 cm^{-1} displayed in Fig. 2 is the region where rather sharp vibrational bands due to isolated OD groups are expected. The OD-IR intensity correlates with the applied D_2O vapor pressure (from top to bottom) and reflects the OD coverage, which has independently been determined by XPS, obtained on the MgO surface after the various water exposures. In addition, this figure displays a clear trend toward higher vibrational frequency as the OD coverage

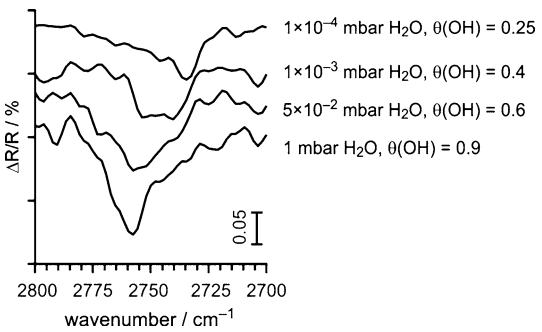

Fig. 2 IRA spectra from MgO(100)/Ag(100) thin films after hydroxylation with D_2O vapor at room temperature. The sample surface has been exposed for 3 min to the D_2O vapor pressure indicated in the Figure. The corresponding OD coverage (θ) in monolayers as determined from XPS is also listed

increases, pointing to some complexity of the structural elements giving rise to these signals. Indeed, the assignment of the IR bands to distinct surface sites on the MgO surface has been a matter of debate for several decades. Here, reference is made to the most recent and most comprehensive computational study that has addressed the vibrational properties of OH groups adsorbed on various low-coordination and defect sites on MgO [70]. It can be concluded from comparison with the computational results that mainly multi-coordinated, isolated OH groups at defect sites such as step edges and kinks are present after hydroxylation at low pressure, whereas the high frequency hydroxyl band seen on the fully hydroxylated surface obtained after exposure to 1 mbar D_2O vapor indicates the formation of mono-coordinated, hydrogen-bond accepter hydroxyls. Controlled variation of the water vapor pressure allows, therefore, distinct hydroxylation states on the MgO surface to be selectively populated. For the investigations into the interaction of gold with hydroxyls that follow, MgO(100) thin films, which have been hydroxylated in 1×10^{-3} mbar D_2O at room temperature for three minutes yielding a hydroxyl coverage of $\sim$0.4 monolayer, have been used.

A most conspicuous evidence for the influence of hydroxyls on nucleation and sintering of Au on MgO(100) is provided by STM. The images displayed in Fig. 3a present the surface morphology for gold deposited at 300 K (left) and after subsequent heating to 600 K (right) on clean MgO(100) (top) and hydroxylated MgO (bottom), respectively [59]. Two main conclusions can be drawn from these results: (i) the density of nucleation sites is much higher on MgO_{hydr}, and (ii) the stability of Au particles towards sintering is greatly enhanced on MgO_{hydr}. This latter point is essential for catalysis because it basically means that the high Au dispersion is maintained at elevated temperature, a result that is corroborated by related CO-TPD studies showing a higher CO adsorption capacity for Au/MgO_{hydr} as compared to Au/MgO(100) [58]. In spite of the importance of this finding, the STM results leave questions about the reason for the enhanced stability of Au on MgO_{hydr} open. Therefore, XPS and IRAS have been applied to obtain more detailed information about the chemical state of Au on MgO_{hydr}. A first hint for a different nucleation process on MgO_{hydr} is provided by the absence of a CO-IRAS signal at 1,850 cm^{-1} typical for single, neutral Au atoms on MgO(100) after Au deposition at 100 K [71]. The sites that give rise to this spectral feature are either not present on MgO_{hydr}, or the Au atoms have been attracted by stronger nucleation sites. Instead, a CO-IRAS band at 2,165 cm^{-1} indicating the formation of cationic (or oxidized) gold was detected and the existence of $Au^{\delta+}$ species was confirmed by XPS showing an Au $4f_{7/2}$ emission at 86.9 eV binding energy (BE), almost 3 eV higher than the

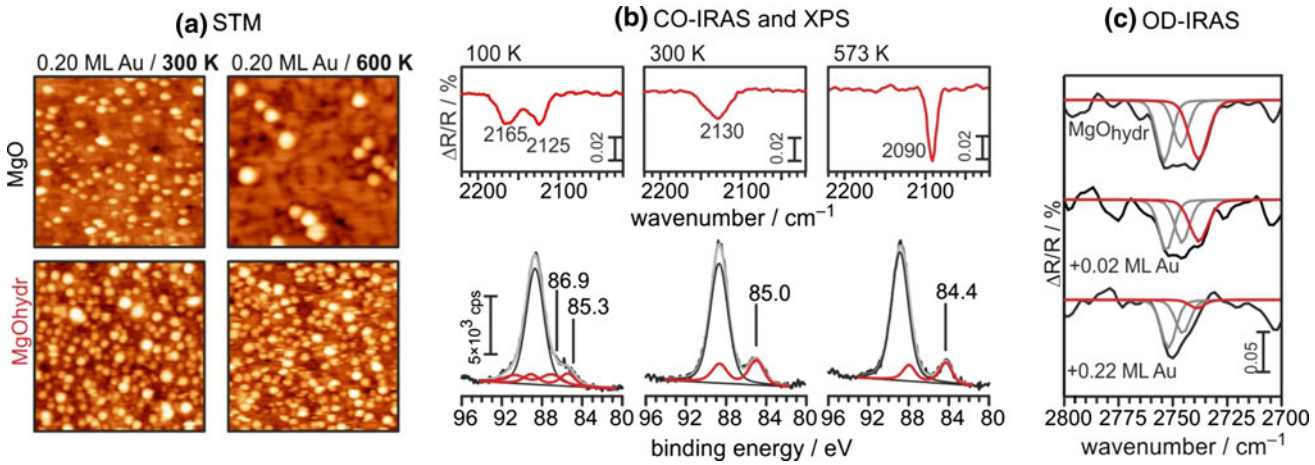

Fig. 3 **a** STM images (50 nm × 50 nm) of 0.2 ML Au evaporated on clean MgO(100) (*top*) and hydroxylated MgO (*bottom*) taken directly after deposition at room temperature (*left*) and after subsequent heating to 600 K (*right*). **b** CO-IRA (*top*) and XP (*bottom*) spectra for 0.05 ML Au deposited on hydroxylated MgO taken directly after Au deposition at 100 K (*left*) and after subsequent heating to 300 K (*middle*) and 573 K (*right*). **c** IRA spectra of the OD spectral detail around 2,750 cm^{-1} taken from hydroxylated MgO (*top*) and after subsequent deposition of 0.02 Au (*middle*) and 0.22 ML Au (*bottom*). [59]

84.0 eV BE of metallic gold (Fig. 3b) [59]. The signatures of cationic gold, although slightly extenuated (smaller CO-IRAS and XPS shifts), remain visible after heating to 300 K, but are gone after annealing to 600 K, where Au is present exclusively in the metallic state (Fig. 3b). A small shift of 0.4 eV to higher BE of the annealed Au on MgO_{hydr} as compared to Au/MgO(100) indicates, however, a remaining final state contribution to the measured BE, which is consistent with the STM result showing the stabilization of smaller particles on MgO_{hydr} (Fig. 3a).

Since hydroxyl groups play obviously a role in the nucleation of Au on MgO_{hydr}, it can be expected that the hydroxyl bands in the IR spectra will also be affected by Au nucleation. The topmost spectrum in Fig. 3c shows the OD region of hydroxylated (D_2O) MgO before Au deposition. The broad OD band can be deconvoluted into three individual signal contributions. The low-frequency signal is depleted upon deposition of Au, while the others do not change in intensity [59]. This result indicates a very specific interaction of Au with hydroxylated MgO that involves only one particular type of surface hydroxyl site. For an assignment of the underlying surface feature we return to Fig. 2, which shows that the low-frequency OD's are the first ones to appear at low hydroxylation pressure. Hydroxyls giving rise to this particular frequency most probably result from water dissociation at the most abundant defects, which are steps. Therefore, hydroxyl groups adsorbed at step edges have been proposed to be the sites of initial gold nucleation on hydroxylated MgO [59]. Based on the STM, IRAS, and XPS findings the sinter stability of Au on MgO_{hydr} is explained by the strong adhesion of Au to the hydroxylated surface, which is a result of the chemical modification (oxidation) of interfacial Au because of the interaction with hydroxyls.

Recent computational studies have addressed the interaction of gold with hydroxylated MgO. Jiang et al. studied the interaction of Au_{10} and Au_{13} with the $Mg(OH)_2$ surface and found strong adhesion of the clusters to the surface. Although the interfacial Au atoms are cationic, the Au clusters are overall negatively charged in these calculations [72]. Jeon et al. [73], on the other hand, considered the possibility that an OH (radical) on the MgO(001) surface spills over onto an adsorbed Au atom resulting in an MgO–Au_1–OH complex . The structure of this complex is reminiscent of MgO–Au_1–CO reported previously [71]. Similar to the CO case, charge flow from the MgO substrate via the gold atom to the OH group is found, and Bader charge analysis confirms that the Au atom is positively charged. Certainly, the hydroxylated MgO surface is a complex system and the models used in the above-mentioned computational studies represent only an approximation to the situation encountered in our experiments. Different morphologies, the influence of hydroxyl/water coverage, as well as the cluster size dependent interaction need to be taken into account in order to obtain better agreement with the experimental results. Nevertheless, the examples described in this section show that steps into a description of metal-support interactions at environmentally complex interfaces are being taken using surface science methodologies. Certainly, the elucidation of atomic scale details requires a strong interplay of experiment and theory. If done so, a better understanding of the processes occurring under non-ideal conditions on model oxide-supported metal particle catalysts can be achieved.

3 Surface Science Approach to Catalyst Preparation

Almost all supported catalysts employed industrially are prepared by wet-chemical methods such as impregnation, deposition–precipitation, spreading, and ion exchange [74]. The fundamental difference with respect to the UHV-surface science approach of preparation of model catalyst surfaces is the nature of the precursor and the way it is transformed into a nanoparticle. Figure 4 highlights the various steps of the surface science and technical catalyst preparation procedures, respectively. In the case of a typical surface science experiment, the catalytically active metal is applied to the clean support by physical vapor deposition (PVD). The impinging metal atoms diffuse on the surface until a stable nuclei is formed either by trapping of atoms at defect sites or by dimerization. Agglomeration and sintering at elevated temperature then leads to the formation of nanoparticles (Fig. 4a). By contrast, the first step of catalyst preparation in a commonly applied wet-chemical procedure consists of the interaction of the support with precursor solutions that contain the metal component in the form of salts or complexes. This is followed by drying, calcination and reduction steps, which are necessary to transform the adsorbed metal precursor into the catalytically active phase (Fig. 4b).

While the processes during the formation of metal nanoparticles on oxide supports are reasonably well understood in the case of the surface science models [10], the complexity of the materials and the lack of suitable analytical techniques render the detailed mechanistic elucidation of the individual steps in technical catalyst preparation a difficult task. Nevertheless, several models have been introduced that catch the essential aspects of the interaction of metal complexes with the support surface at the oxide-liquid interface [75]. To mention here are the "strong electrostatic adsorption" model [76] (based on pioneering work by Brunelle [77]), which considers mainly an electrostatic adsorption mechanism of charged precursor complexes, and the "interfacial coordination chemistry" approach [78], which includes strong chemical bonding (grafting) of the precursor complexes to the support in addition to electrostatic adsorption. With these models it is possible to reasonably simulate the metal uptake as a function of precursor solution parameters (pH, metal concentration) [79]. The least understood process in technical catalyst preparation seems to be the transformation of the precatalyst into the raw catalyst, i.e. the decomposition of the adsorbed precursor during the calcination step. This was highlighted by Richard G. Finke in a recent review paper that discusses the existing literature in this area and where the following statement can be found: "Overall, surprisingly little is known about the mechanism(s) of formation of the desired size, shape and compositionally controlled supported nanoparticle catalysts" [80]. New developments in the field of in situ experimental techniques, such as magnetic resonance imaging [81], the X-ray differential pair distribution function method [82], or environmental transmission electron microscopy [83], promise to provide new insight into these processes.

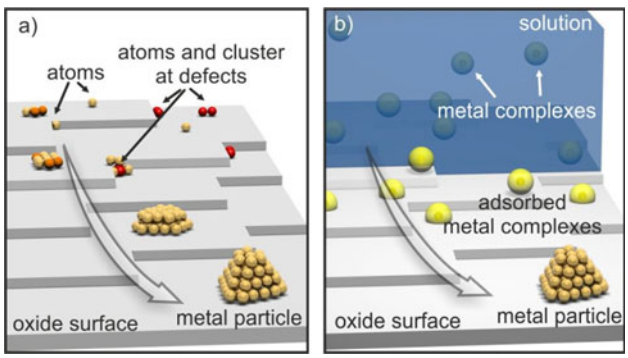

Fig. 4 Schematic representation of the individual stages of preparation of **a** a model catalyst in UHV, and **b** a technical catalyst

Surface scientists have in the past undertaken several attempts to mimic catalyst preparation using flat substrates. For example, in an early work by Ertl et al. the preparation and characterization of vanadia species on a TiO_2 substrate that was obtained by oxidation of a thin Ti layer on a support was described [84]. Later on, several reports about carbon-based Pt catalysts investigated by STM appeared from the groups of Wolf [85, 86] and Baiker [87, 88].

During the last 20 years, the group of Hans Niemantsverdriet has studied the preparation of flat model catalysts by applying wet-chemical preparation protocols, in particular the spin-coating technique, to amorphous silica or alumina substrates [89–91].

Reports on the elucidation of the precursor interaction with single-crystalline oxide substrates should not be left out. These include, e.g., an in situ investigation of the adsorption of Pt-tetraammine complexes on a quartz(100) surface using surface X-ray reflectivity [92], and a very recent report on the precipitation of Ni on α-Al_2O_3 investigated with grazing-incidence X-ray absorption [93]. Despite the wealth of information obtained with the above-mentioned surface science approaches, most of them have also limitations: The use of insulating bulk single-crystal oxides imposes some restrictions as to the applicability of standard surface science methods, and with thin, amorphous oxide films (obtained for example by surface oxidation of a Si wafer) as substrates, a good part of the morphological control is lost.

We have recently started to study catalyst preparation using thin, single-crystalline oxide films grown on metallic substrates as supports, which represent promising alternatives for surface science investigations of catalyst preparation

[94, 95]. Our studies used 10 nm thin $Fe_3O_4(111)$ films grown on Pt(111) as substrate. An STM image of a freshly prepared $Fe_3O_4(111)$ film, which has subsequently been transferred into air for STM imaging, is presented in Fig. 5a. The observed morphology of this surface compares well with previous UHV-STM studies, and occasionally, atomic resolution of the topmost iron layer could be achieved (see inset in Fig. 5a), demonstrating the good environmental stability of the oxide film surface. With $Fe_3O_4(111)$/Pt(111) as support, we have studied the preparation of supported Pd nanoparticles using $PdCl_2$ as a precursor. The speciation of $PdCl_2$ in aqueous solutions has been the subject of intense research in the past. In strongly acidic conditions, the tetrachloro complex $PdCl_4^{2-}$ is the most abundant species. Upon hydrolysis, the chlorine ligands are gradually replaced by aqua or hydroxo ligands, leading finally to $Pd(OH)_4^{2-}$ species in strongly basic medium [96, 97]. Neutral Pd complexes of the kind $[PdCl_2(H_2O)_2]$ are formed at an intermediate stage of hydrolysis. These complexes are most probably responsible, because of their tendency for polymerization (→polynuclear Pd-hydroxo complexes, PHC), for the formation of colloidal particles [98], seen with the appearance of the dark brown color of the Pd solution (see Fig. 5e). The pH at which formation of PHC's sets in can be slightly varied by changing the Pd^{2+} and Cl^- concentration.

The strong influence of the solution pH on the Pd loading and the particle morphology is demonstrated by means of the STM images displayed in Fig. 5b–e. These images were obtained following exposure of the $Fe_3O_4(111)$ films to $PdCl_2$ precursor solutions exhibiting different solution pH (as indicated in Fig. 5), and subsequent thermal treatment at 600 K in UHV, which transforms the adsorbed Pd precursor into Pd particles. First consider the samples prepared with the low pH solutions (pH 1.3–2.5), where the influence of PHC's can be excluded. The trend toward higher Pd loading and slightly increasing Pd particle size with increasing pH is obvious and in agreement with results obtained for similar preparations carried out with powder samples [79, 99]. Within the "strong electrostatic adsorption" model, which seems to be applicable for the given conditions (negatively charged precursor and positively charge support surface, $PZC(Fe_3O_4) \sim$ pH 6.5), the suppression of Pd precursor adsorption at low pH, which results in low Pd loading, is typically explained by the lowering of the equilibrium adsorption constant as an effect of the higher ionic strength of the strongly acidified precursor solution [100].

While small and homogeneously distributed Pd particles are formed following exposure to the low pH solutions, a high Pd loading and large Pd particles are obtained if the pH 4.7 precursor solution is applied. At first glance, this result might be related to the adsorption of colloidal particles present in the precursor solution. However, deposited particles could not be identified by STM directly after deposition. Therefore, a different adsorption mechanism for the Pd precursor needs to be considered at this pH conditions. Since at pH 4.7 the Fe_3O_4 surface is essentially uncharged and a considerable fraction of the solution species is charge-neutral, a strong chemical interaction via hydrolytic adsorption of the precursor complexes could be the reason for the high Pd loading. With the basic pH 10 precursor solution the Pd loading decreased again and a particle size distribution that is more homogeneous as

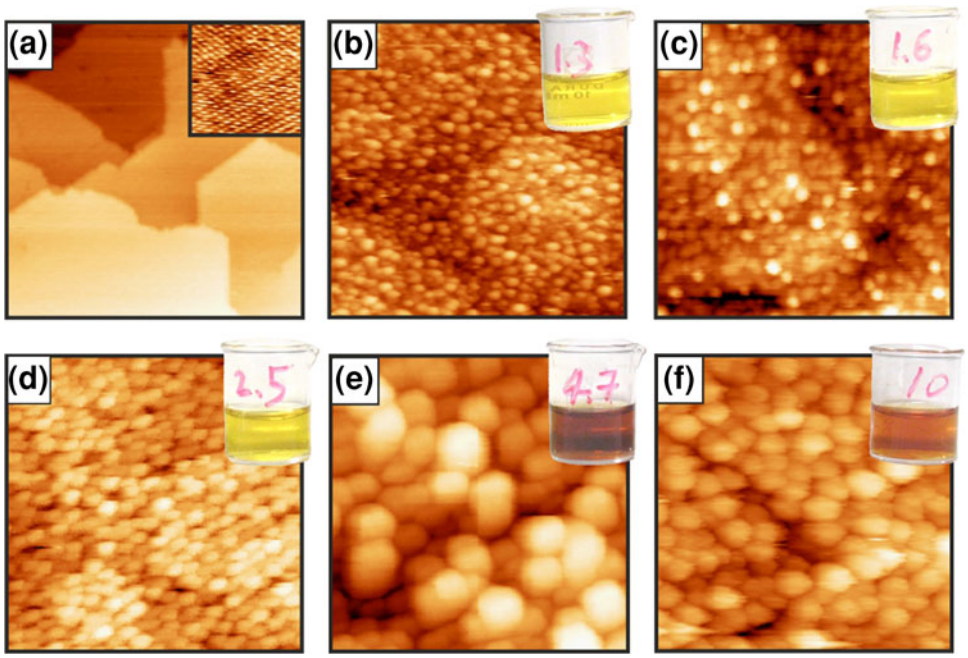

Fig. 5 **a** STM images (100 nm × 100 nm) of a $Fe_3O_4(111)$/Pt(111) sample prepared in UHV and transferred into air. The *inset* shows an atomically resolved STM image from a terrace of the sample surface (8 nm × 8 nm). **b–f** STM images (75 nm × 75 nm) of Pd/Fe_3O_4 samples obtained by exposure of freshly prepared $Fe_3O_4(111)$ to $PdCl_2$ precursor solutions (**b–e**: 5 mM $PdCl_2$, **f**: 2mM $PdCl_2$, pH as indicated in the figure, deposition time: 60 min.) and subsequent thermal treatment at 600 K in UHV conditions

compared to the one obtained with the pH 4.7 precursor solution was obtained. Since both the oxide surface and the solution complexes are negatively charged in this case, electrostatic adsorption is believed to play a negligible role and the adsorption of Pd occurs mainly via hydrolytic adsorption of the Pd-hydroxo complexes on the surface hydroxyl groups.

More detailed studies regarding the stepwise decomposition of the adsorbed precursors into metallic nanoparticles were conducted with samples prepared by exposure to pH 1.3 and pH 10 precursor solutions, respectively [94, 95]. As an example, we show the results obtained with the alkaline precursor solution in Fig. 6a (STM) and Fig. 6b (XPS). An STM image of the $Fe_3O_4(111)$ surface following exposure to the precursor solution (2 mM $PdCl_2$, pH 10) and subsequent water rinsing and drying shows an apparently "clean" oxide surface with the typical morphological features of $Fe_3O_4(111)$ (Fig. 6a, top). However, the corresponding XPS spectrum confirms the presence of Pd on this surface (Fig. 6b, top). Obviously, the adsorbed precursor complexes are homogeneously distributed across the surface and cannot be individually resolved in STM. The two Pd $3d_{5/2}$ photoemission signals identified at 337.8 eV and 336.5 eV BE can be assigned to Pd-hydroxo and PdO species, respectively. It has to be mentioned that the high BE component was found to be sensitive to X-ray irradiation, and the PdO component identified at this stage of the preparation results most probably from X-ray induced decomposition of the Pd-hydroxide into PdO. Only mild drying at 390 K completely changes the surface morphology, which displays now the presence of small particles with an average diameter of 2.5–3 nm (Fig. 6a, middle). This morphological change is accompanied by an almost complete transformation of the adsorbed Pd-hydroxide precursor into PdO, as deduced from the loss of the high BE component in XPS and the concurrent increase of the 335.9 eV feature (Fig. 6b, middle). Finally, fully reduced Pd particles (particle diameter: 3–7 nm) are found after further thermal treatment at 600 K (Fig. 6a and b, bottom). These particles contain some carbon contamination remaining from the preparation process, which can be eliminated by oxidation at 500 K in 1×10^{-6} mbar O_2. Subsequent reduction in CO atmosphere restores the metallic state, which then presents CO-IRAS signatures typical for supported Pd nanoparticles (Fig. 6c) with two bands arising, respectively, from on-top bound (2,105 cm^{-1}) and bridge-bonded CO (1,990 cm^{-1}) [101, 102]. Alternatively, the final reduction step was performed in H_2 instead of CO atmosphere, which led to the formation of bimetallic Pd-Fe particles due to strong metal-support interaction (SMSI). This modification can be easily understood on the basis of the catalytic action of Pd in providing H atoms for reduction of the Fe_3O_4 support via H_2 dissociation

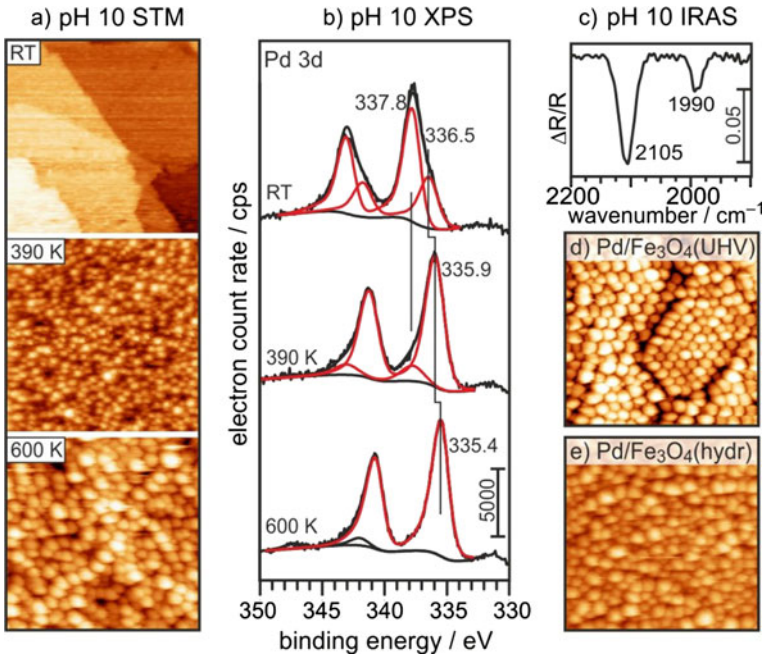

Fig. 6 **a** STM images (100 nm × 100 nm) and **b** corresponding Pd 3d photoemission spectra of a $Fe_3O_4(111)$/Pt(111) thin film surface acquired after exposure to Pd precursor solution (5 mM $PdCl_2$, pH 10) and subsequent drying (RT, *top*), after drying at 390 K (*middle*), and subsequent heating to 600 K (*bottom*). **c** IRA spectrum of a Pd/$Fe_3O_4(111)$ model catalyst prepared by exposure to pH 10 $PdCl_2$ precursor solution taken after adsorption of CO at 80 K. **d** STM image (100 nm × 100 nm) of Pd/$Fe_3O_4(111)$ prepared by physical vapor deposition of Pd in UHV. **e** STM image (100 nm × 100 nm) of Pd/$Fe_3O_4(111)$ prepared by physical vapor deposition of Pd onto a $Fe_3O_4(111)$ surface modified by treatment with NaOH solution. [95]

and H spill-over. Iron atoms from the reduced support then migrate into the Pd particles.

An important question to ask at this point is whether or not the morphology of a model catalyst prepared by wet-chemical procedures as described above differs from that of a corresponding model catalyst prepared exclusively in UHV. In other words, does the nature of the precursor (single atoms in UHV vs. metal complexes in solution) or the support properties (clean surface in UHV vs. a surface modified by exposure to precursor solution) affect the properties of the activated model catalyst? In order to answer this question two additional $Pd/Fe_3O_4(111)$ model catalysts were prepared: one, where Pd was deposited onto a clean $Fe_3O_4(111)$ support in UHV by vapor deposition (Pd/Fe_3O_4(UHV), Fig. 6d), and another one, where Pd was deposited by vapor deposition onto a $Fe_3O_4(111)$ surface following a treatment with NaOH (pH 12) solution (Pd/Fe_3O_4(hydr), Fig. 6e). The NaOH treatment was applied in order to achieve a surface functionality comparable to the solution deposition experiment. Inspection of the corresponding STM images (Figs. 6d and 6e) reveals differences between the two samples with respect to the arrangement of the Pd particles and the particle size distribution. While the Pd particles are uniform in size and arranged in an almost perfect hexagonal array on the clean $Fe_3O_4(111)$ surface, the surface order is lost on the pre-treated Fe_3O_4 surface and a deviation from the normal particle size distribution is apparent. Most notably, the morphology of the Pd/Fe_3O_4(hydr) sample (Fig. 6e) closely resembles that of the model catalyst prepared by deposition of Pd from the pH 10 precursor solution (Fig. 6a, bottom). This finding suggests that in the present case the morphology of the activated model catalyst is mainly governed by the interfacial properties, and not by the nature of the precursor. The more heterogeneous sintering of Pd particles on the modified surfaces is attributed to the presence of hydroxyl groups and the existence of a variety of adsorption sites with differing Pd adhesion properties [95].

Finally, the activity of the model catalysts in CO oxidation was investigated with temperature programmed reaction. Particular attention was paid to the differences between the regular model catalyst (obtained by reduction in CO atmosphere) and the one in the SMSI state (obtained by reduction in H_2 atmosphere). Since Fe_3O_4 is a reducible oxide with oxygen storage potential, the involvement of lattice oxygen in CO oxidation (→Mars-van Krevelen type mechanism) was first explored in a CO-TPD run without additional oxygen exposure. Indeed, and in agreement with earlier studies [103], the sample activated by oxidation and CO reduction gave rise to a CO_2 signal at around 500 K (Fig. 7). By contrast, no CO_2 could be detected from the SMSI sample. The weak bonding of CO to the bimetallic particles can be ruled out as explanation for the lack of reactivity on the basis of the results for the CO oxidation reaction described below. It is rather the unavailability of lattice oxygen in the reduced near-surface regions of the reduced support that is responsible for the lack of activity in this type of reaction. If molecular oxygen is predosed, enhanced CO_2 production is observed on both samples (Fig. 7, filled circles). It is noted that the CO_2 signal arising from the sample activated by oxidation and subsequent reduction in CO appears to be the sum of two contributions: one from a reaction of CO with lattice oxygen exhibiting a maximum at around 500 K, and the other one from the reaction of CO with dissociated oxygen on the Pd particles, which extends from 400 to 550 K. Since the former contribution is missing on the sample prepared by reduction in H_2 atmosphere, only the catalytic CO oxidation path is observed in this case.

To summarize, the results presented above have clearly demonstrated the feasibility of surface science investigations related to catalyst preparation by utilizing single-crystalline, thin oxide films as supports. Various steps of the catalyst preparation procedure, from the clean support surface, via decomposition of the precursor, and finally to characterization of the activated model catalyst, could be analyzed with typical surface science spectroscopic and microscopic techniques. A future challenge in these studies will be to analyze in detail the initial interaction between the oxide support and the metal precursor at the oxide-liquid interface with in situ microscopic and spectroscopic techniques.

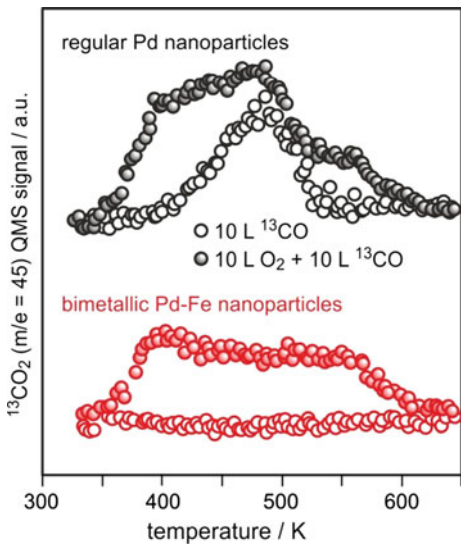

Fig. 7 $^{13}CO_2$ TPD spectra obtained from $Pd/Fe_3O_4(111)$ model catalysts activated by reduction in CO atmosphere (*top*) and H_2 atmosphere (*bottom*), after dosing ^{13}CO (*open circles*) or $^{13}CO + O_2$ (*filled circles*) at room temperature

4 Concluding Remarks

Surface science investigations have strongly contributed to our understanding of catalytically relevant processes. The strength of the surface science approach is based on the possibility to have ultimate control over the morphology of the model surfaces (metal single crystals), allowing structure–reactivity relationships to be established. New challenges in the characterization and interpretation of surface functionality arise as we move on to more complex surfaces and interfaces. In this article, we highlighted recent surface science work in the field of oxide-supported metal nanoparticle model catalysts that put emphasis on the influence of hydroxylated supports on the properties of metals deposited from the vapor phase, and on catalyst preparation using wet-chemical procedures. The examples discussed herein document the progress that has been made over the last years in the description of these complex interface phenomena.

Acknowledgments We thank all present and previous coworkers who contributed to the work presented in this article, in particular Matthew A. Brown, Esther Carrasco, Yuichi Fujimori, Hui-Feng Wang and William E. Kaden. Financial support by the Fonds der Chemischen Industrie and the Deutsche Forschungsgemeinschaft through the Cluster of Excellence UNICAT (administered by TU Berlin) is gratefully acknowledged.

References

1. Ertl G (1994) Surf Sci 299:742
2. Marsh AL, Ribeiro FH, Somorjai GA (2008) In: Ertl G, Knözinger H, Schüth F, Weitkamp J (eds) Handbook of heterogeneous catalysis. VCH, Weinheim, p 1259
3. Zaera F (2001) Prog Surf Sci 69:1
4. Somorjai GA, York RL, Butcher D, Park JY (2007) Phys Chem Chem Phys 9:3500
5. Freund HJ, Kuhlenbeck H, Libuda J, Rupprechter G, Bäumer M, Hamann H (2001) Top Catal 15:201
6. Gunter PLJ, Niemantsverdriet JW, Ribeiro FH, Somorjai GA (1997) Catal Rev-Sci Eng 39:77
7. Rupprechter G (2007) In: Gates BC and Knözinger H (eds) Advances in catalysis. Elsevier Academic Press Inc, San Diego, p 133
8. Bluhm H, Hävecker M, Knop-Gericke A, Kiskinova M, Schlögl R, Salmeron M (2007) MRS Bull 32:1022
9. Hendriksen BLM, Frenken JWM (2002) Phys Rev Lett 89: 046101
10. Campbell CT (1997) Surf Sci Rep 27:1
11. Freund HJ (1997) Angew Chem Int Ed 36:452
12. Bäumer M, Freund HJ (1999) Prog Surf Sci 61:127
13. Henry CR (1998) Surf Sci Rep 31:235
14. McClure SM, Goodman DW (2011) Top Catal 54:349
15. Freund HJ, Goodman DW (2008) In: Ertl G, Knözinger H, Schüth F and Weitkamp J (eds) Handbook of heterogeneous catalysis. VCH, Weinheim, p 1309
16. Sterrer M, Risse T, Heyde M, Rust HP, Freund HJ (2007) Phys Rev Lett 98:206103
17. Yulikov M, Sterrer M, Heyde M, Rust HP, Risse T, Freund HJ, Pacchioni G, Scagnelli A (2006) Phys Rev Lett 96:146804
18. Sterrer M, Fischbach E, Risse T, Freund HJ (2005) Phys Rev Lett 94:186101
19. Sterrer M, Heyde M, Novicki M, Nilius N, Risse T, Rust HP, Pacchioni G, Freund HJ (2006) J Phys Chem B 110:46
20. Sterrer M, Yulikov M, Fischbach E, Heyde M, Rust HP, Pacchioni G, Risse T, Freund HJ (2006) Angew Chem Int Ed 45:2630
21. Boehm H-P, Knözinger H (1983) In: Anderson JR and Boudart M (eds) Catalysis science and technology. Springer, Berlin, p 39
22. Carrasco J, Illas F, Lopez N (2008) Phys Rev Lett 100:016101
23. Scamehorn CA, Harrison NM, McCarthy MI (1994) J Chem Phys 101:1547
24. Liu LM, Zhang CJ, Thornton G, Michaelides A (2010) Phys Rev B 82:161415
25. Hugenschmidt MB, Gamble L, Campbell CT (1994) Surf Sci 302:329
26. Kurtz RL, Stockbauer R, Madey TE, Roman E, Desegovia JL (1989) Surf Sci 218:178
27. Ketteler G, Yamamoto S, Bluhm H, Andersson K, Starr DE, Ogletree DF, Ogasawara H, Nilsson A, Salmeron M (2007) J Phys Chem C 111:8278
28. Zhang Z, Fenter P, Sturchio NC, Bedzyk MJ, Machesky ML, Wesolowski DJ (2007) Surf Sci 601:1129
29. Liu P, Kendelewicz T, Gordon GE, Parks GA (1998) Surf Sci 412–13:287
30. Carrasco E, Brown MA, Sterrer M, Freund HJ, Kwapien K, Sierka M, Sauer J (2010) J Phys Chem C 114:18207
31. Mejias JA, Berry AJ, Refson K, Fraser DG (1999) Chem Phys Lett 314:558
32. Eng PJ, Trainor TP, Brown GE, Waychunas GA, Newville M, Sutton SR, Rivers ML (2000) Science 288:1029
33. Wang XG, Chaka A, Scheffler M (2000) Phys Rev Lett 84:3650
34. Rohrbach A, Hafner J, Kresse G (2004) Phys Rev B 70:125426
35. Yamamoto S, Kendelewicz T, Newberg JT, Ketteler G, Starr DE, Mysak ER, Andersson KJ, Ogasawara H, Bluhm H, Salmeron M, Brown GE, Nilsson A (2010) J Phys Chem C 114:2256
36. Hass KC, Schneider WF, Curioni A, Andreoni W (1998) Science 282:265
37. Wendt S, Schaub R, Matthiesen J, Vestergaard EK, Wahlstrom E, Rasmussen MD, Thostrup P, Molina LM, Laegsgaard E, Stensgaard I, Hammer B, Besenbacher F (2005) Surf Sci 598:226
38. Bikondoa O, Pang CL, Ithnin R, Muryn CA, Onishi H, Thornton G (2006) Nature Mater 5:189
39. Matthey D, Wang JG, Wendt S, Matthiesen J, Schaub R, Laegsgaard E, Hammer B, Besenbacher F (2007) Science 315:1692
40. Wang JG, Hammer B (2006) Phys Rev Lett 97:136107
41. Henderson MA, Epling WS, Peden CHF, Perkins CL (2003) J Phys Chem B 107:534
42. Libuda J, Frank M, Sandell A, Andersson S, Bruhwiler PA, Bäumer M, Martensson N, Freund HJ (1997) Surf Sci 384:106
43. Starr DE, Diaz SF, Musgrove JE, Ranney JT, Bald DJ, Nelen L, Ihm H, Campbell CT (2002) Surf Sci 515:13
44. Günster J, Krischok S, Kempter V, Stultz J, Goodman DW (2002) Surf Rev Lett 9:1511
45. Heemeier M, Frank M, Libuda J, Wolter K, Kuhlenbeck H, Bäumer M, Freund HJ (2000) Catal Lett 68:19
46. Heemeier M, Stempel S, Shaikhutdinov SK, Libuda J, Bäumer M, Oldman RJ, Jackson SD, Freund HJ (2003) Surf Sci 523:103
47. Chambers SA, Droubay T, Jennison DR, Mattsson TR (2002) Science 297:827
48. Niu C, Shepherd K, Martini D, Tong J, Kelber JA, Jennison DR, Bogicevic A (2000) Surf Sci 465:163
49. Lazzari R, Jupille J (2005) Phys Rev B 71:045409
50. Fu Q, Wagner T, Rühle M (2006) Surf Sci 600:4870

51. Jensen MCR, Venkataramani K, Helveg S, Clausen BS, Reichling M, Besenbacher F, Lauritsen JV (2008) J Phys Chem C 112:16953
52. Lodziana Z, Norskov JK (2001) J Chem Phys 115:11261
53. Sanz JF, Hernandez NC (2005) Phys Rev Lett 94:016104
54. Vayssilov GN, Gates BC, Rösch N (2003) Angew Chem Int Ed 42:1391
55. Vayssilov GN, Rösch N (2005) Phys Chem Chem Phys 7:4019
56. Hu CH, Chizallet C, Mager-Maury C, Corral-Valero M, Sautet P, Toulhoat H, Raybaud P (2010) J Catal 274:99
57. Weber WA, Gates BC (1997) J Phys Chem B 101:10423
58. Brown MA, Carrasco E, Sterrer M, Freund HJ (2010) J Am Chem Soc 132:4064
59. Brown MA, Fujimori Y, Ringleb F, Shao X, Stavale F, Nilius N, Sterrer M, Freund HJ (2011) J Am Chem Soc 133:10668
60. Bond GC, Thompson DT (2000) Gold Bulletin 33:41
61. Kung MC, Davis RJ, Kung HH (2007) J Phys Chem C 111:11767
62. Cunningham DAH, Vogel W, Haruta M (1999) Catal Lett 63:43
63. Cunningham DAH, Vogel W, Kageyama H, Tsubota S, Haruta M (1998) J Catal 177:1
64. Jia CJ, Liu Y, Bongard H, Schüth F (2010) J Am Chem Soc 132:1520
65. Takei T, Okuda I, Bando KK, Akita T, Haruta M (2010) Chem Phys Lett 493:207
66. Qiao BT, Zhang J, Liu LQ, Deng YQ (2008) Appl Catal A 340:220
67. Veith GM, Lupini AR, Dudney NJ (2009) J Phys Chem C 113:269
68. Wlodarczyk R, Sierka M, Kwapien K, Sauer J, Carrasco E, Aumer A, Gomes JF, Sterrer M, Freund HJ (2011) J Phys Chem C 115:6764
69. Carrasco E, Aumer A, Gomes JF, Fujimori Y, Sterrer M (2013) Chem Commun. doi:10.1039/c2cc37148k
70. Chizallet C, Costentin G, Che M, Delbecq F, Sautet P (2007) J Am Chem Soc 129:6442
71. Sterrer M, Yulikov M, Risse T, Freund HJ, Carrasco J, Illas F, Di Valentin C, Giordano L, Pacchioni G (2006) Angew Chem Int Ed 45:2633
72. Jiang DE, Overbury SH, Dai S (2011) J Phys Chem Lett 2:1211
73. Jeon J, Soon A, Yeo JN, Park J, Hong S, Cho K, Yu BD (2012) J Phys Soc Jpn 81:054601
74. Gallei EF, Hesse M, Schwab E (2008) In: Ertl G, Knözinger H, Schüth F and Weitkamp J (eds) Handbook of heterogeneous catalysis. VCH, Weinheim, p 57
75. Regalbuto JR (ed) (2007) Catalyst preparation—science and engineering. CRC Press, Boca Raton
76. Hao X, Spieker WA, Regalbuto JR (2003) J Colloid Interface Sci 267:259
77. Brunelle JP (1978) Pure Appl Chem 50:1211
78. Lambert JF, Che M (2000) J Mol Catal A-Chem 162:5
79. Jiao L, Regalbuto JR (2008) J Catal 260:329
80. Mondloch JE, Bayram E, Finke RG (2012) J Mol Catal A-Chem 355:1
81. Espinosa-Alonso L, Lysova AA, Peinder P, de Jong KP, Koptyug IV, Weckhuysen BM (2009) J Am Chem Soc 131:6525
82. Chupas PJ, Chapman KW, Jennings G, Lee PL, Grey CP (2007) J Am Chem Soc 129:13822
83. Banerjee R, Crozier PA (2012) J Phys Chem C 116:11486
84. Nickl J, Schlögl R, Baiker A, Knözinger H, Ertl G (1989) Catal Lett 3:379
85. Yeung KL, Wolf EE (1991) J Vac Sci Technol B 9:798
86. Yeung KL, Wolf EE (1992) J Catal 135:13
87. Atamny F, Baiker A (1998) Appl Catal A 173:201
88. Atamny F, Duff D, Baiker A (1995) Catal Lett 34:305
89. Niemantsverdriet JW, Engelen AFP, de Jong AM, Wieldraaijer W, Kramer GJ (1999) Appl Surf Sci 144–45:366
90. Thune PC, Niemantsverdriet JW (2009) Surf Sci 603:1756
91. Vanhardeveld RM, Gunter PLJ, Vanijzendoorn LJ, Wieldraaijer W, Kuipers EW, Niemantsverdriet JW (1995) Appl Surf Sci 84:339
92. Park C, Fenter PA, Sturchio NC, Regalbuto JR (2005) Phys Rev Lett 94:076104
93. Tougerti A, Llorens I, D'Acapito F, Fonda E, Hazemann JL, Joly Y, Thiaudiere D, Che M, Carrier X (2012) Angew Chem Int Ed 51:7697
94. Wang HF, Ariga H, Dowler R, Sterrer M, Freund HJ (2012) J Catal 286:1
95. Wang HF, Kaden WE, Dowler R, Sterrer M, Freund HJ (2012) Phys Chem Chem Phys 14:11525
96. Milic NB, Bugarcic ZD (1984) Transit Met Chem 9:173
97. van Middlesworth JM, Wood SA (1999) Geochim Cosmochim Acta 63:1751
98. Didillon B, Merlen E, Pages T, Uzio D (1998) Stud Surf Sci Catal 118:41
99. Regalbuto JR, Navada A, Shadid S, Bricker ML, Chen Q (1999) J Catal 184:335
100. Shah AM, Regalbuto JR (1994) Langmuir 10:500
101. Rainer DR, Wu MC, Mahon DI, Goodman DW (1996) J Vac Sci Technol A 14:1184
102. Wolter K, Seiferth O, Kuhlenbeck H, Bäumer M, Freund HJ (1998) Surf Sci 399:190
103. Meyer R, Shaikhutdinov SK, Freund HJ (2004) Z Phys Chemie 218:905